Science of the Total Environment 934 (2024) 173236

Contents lists available at ScienceDirect

Science of the Total Environment

journal homepage: www.elsevier.com/locate/scitotenv

Hazard assessment of nanoplastics is driven by their surface-functionalization. Effects in human-derived primary endothelial cells

Joan Martín-Pérez [a], Aliro Villacorta [a,b], Gooya Banaei [a], Michelle Morataya-Reyes [a], Alireza Tavakolpournegari [a], Ricard Marcos [a,*], Alba Hernández [a,*], Alba García-Rodriguez [a,*]

[a] Group of Mutagenesis, Department of Genetics and Microbiology, Faculty of Biosciences, Universitat Autònoma de Barcelona, Cerdanyola del Vallès 08193, Spain
[b] Facultad de Recursos Naturales Renovables, Universidad Arturo Prat, Iquique, Chile

HIGHLIGHTS

- Polystyrene nanoplastics with different surface functionalizations were used.
- Primary human umbilical vein endothelial cells exposed at different times were used.
- Cell internalization dynamics were evaluated using different methodological approaches.
- Aminated shows a lower tendency to internalize than pristine and carboxylated forms.
- All forms triggered oxidative stress and genotoxicity responses.

GRAPHICAL ABSTRACT

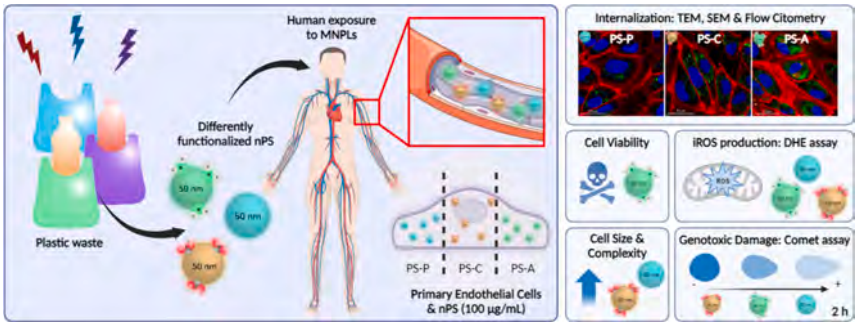

ARTICLE INFO

Editor: Susanne Brander

Keywords:
HUVEC
Polystyrene nanoplastics
Functionalization
Internalization
Genotoxicity

ABSTRACT

During plastic waste degradation into micro/nanoplastics (MNPLs) their physicochemical characteristics including surface properties (charge, functionalization, biocorona, *etc.*) can change, potentially affecting their biological effects. This paper focuses on the surface functionalization of MNPLs to determine if it has a direct impact on the toxicokinetic and toxicodynamic interactions in human umbilical vein endothelial cells (HUVECs), at different exposure times. Pristine polystyrene nanoplastics (PS-NPLs), as well as their carboxylated (PS-C-NPLs) and aminated (PS-A-NPLs) forms, all around 50 nm, were used in a wide battery of toxicological assays. These assays encompassed evaluations on cell viability, cell internalization, induction of intracellular reactive oxygen species (iROS), and genotoxicity. The experiments were conducted at a concentration of 100 µg/mL, chosen to ensure a high internalization rate across all treatments while maintaining a sub-toxic concentration. Our results show that all PS-NPLs are internalized by HUVECs, but the internalization dynamic depends on the particle's functionalization. PS-NPLs and PS-C-NPLs internalization modify the morphology of the cell increasing its inner complexity/granularity. Regarding cell toxicity, only PS-A-NPLs reduced cell viability. Intracellular ROS was induced by the three different PS-NPLs but at different time points. Genotoxic damage was induced by the three PS-NPLs at short exposures (2 h), but not for PS-C-NPLs at 24 h. Overall, this study suggests that the

* Corresponding authors at: Group of Mutagenesis, Department of Genetics and Microbiology, Faculty of Biosciences, Universitat Autònoma de Barcelona, Campus of Bellaterra, 08193 Cerdanyola del Vallès, Spain.
E-mail addresses: ricard.marcos@uab.cat (R. Marcos), alba.hernandez@uab.cat (A. Hernández), alba.garcia.rodriguez@uab.cat (A. García-Rodriguez).

https://doi.org/10.1016/j.scitotenv.2024.173236
Received 4 January 2024; Received in revised form 14 April 2024; Accepted 12 May 2024
Available online 17 May 2024

toxicological effects of PSNPLs on HUVEC cells are surface-dependent, highlighting the relevance of using human-derived primary cells as a target.

1. Introduction

Plastic waste has become a serious environmental problem due to the exponential production of plastic over the past few decades. In the last 60 years, plastic production has increased by >20-fold, resulting in an annual generation of approximately 400 million tons of plastic, with projections indicating a dramatic increase in the coming years (Bajt, 2021). Due to their characteristics, including low-cost production, high durability, and versatility, plastics are used for multiple purposes, such as packaging, cosmetics, building, and medical applications, among others (Domenech and Marcos, 2021). Regrettably, >80 % of these plastics are not adequately recycled and are being released into the natural environment, where they can persist for centuries due to their slow degradation rate (Kik et al., 2020; Lampitt et al., 2023). Exposure to environmental factors such as ultraviolet radiation, wave action, and various physicochemical and biological processes triggers the aging and fragmentation of plastics into smaller particles known as microplastics and even finer nanoplastics (Yee et al., 2021; Shi et al., 2022). These micro/nanoplastics (MNPLs) are contaminating all environmental compartments, including the hydrosphere, atmosphere, and biosphere (Pradel et al., 2023). During the weathering process, MNPLs undergo alterations in their surface properties, acquiring various functional groups such as amino or carboxyl, which in turn influence their properties, including net charge (Alimi et al., 2022).

Studies have highlighted the pathways through which environmental MNPLs can infiltrate the human body, encompassing inhalation, ingestion, and skin contact (Rubio et al., 2020a). Once inside the human body, owing to their minute size, MNPLs possess the potential to breach biological membranes, gaining access to the bloodstream (Yee et al., 2021). Notably, in the case of pulmonary exposure *via* inhalation, the lung's exceptionally thin tissue barrier, measuring <1 μm, facilitates the penetration of nanoscale particles into the capillary bloodstream (Lehner et al., 2019). The translocation of nanoplastics across the gastrointestinal tract through ingestion has been established in different model organisms, suggesting a comparable mechanism in human physiology. This phenomenon has been validated *in vitro* for polystyrene nanoparticles using both simple intestine cell monocultures and more complex human intestinal models including two/three different cell types (Lehner et al., 2019). Concerning dermal exposure, potential entry routes have been delineated, encompassing hair follicles, sweat gland exits, and compromised areas of the skin (Schneider et al., 2009). Substantiating the capacity of nanoplastics to traverse biological barriers and access the bloodstream, a groundbreaking biomonitoring study has revealed the presence of MNPLs (≥700 nm) in whole blood samples from 22 healthy volunteers (Leslie et al., 2022). Intriguingly, among the most prevalent plastics environmentally identified polystyrene, alongside polyethylene terephthalate and polyethylene have been reported (Jeong et al., 2024). The lumen of the human blood vessel is covered by a thin layer of endothelial cells (ECs). These cells are of particular interest in nanotoxicological studies as they function as the first contact for MNPLs entering the bloodstream. Additionally, ECs play a pivotal role in numerous processes, including the regulation of blood vessel tone and monocyte recruitment. Dysregulation of these processes has been implicated in the development of cardiovascular diseases, including atherosclerosis (Xue et al., 2023). Consequently, the study of the effects of nanoplastics on endothelial cells is of major concern nowadays mainly after the results showing that nanoplastics can induce vascular endothelial injury and coagulation dysfunction in mice (Wang et al., 2023), and the proposal of MNPLs as a potential cardiovascular risk factor (Zhu et al., 2023). Among endothelial cells, primary isolated human umbilical vein endothelial cells (HUVECs) are the most widely utilized in research, due to the accessibility of human umbilical veins and their ready availability from commercial sources (Cao et al., 2017).

Different studies have been conducted to investigate the effects of nanoplastics on HUVECs, commonly using nanopolystyrene particles as a model of nanoplastic. These studies have shown that PS-NPLs can induce cytotoxicity, intracellular reactive oxygen species (iROS) production, and autophagy, potentially affecting human health (Fu et al., 2022; Lu et al., 2022). Nevertheless, none of these studies have aimed to elucidate the implications of distinct surface properties of nanoplastics in HUVECs, nor explored the genotoxic potential of these particles. Thus, our study aimed to elucidate the potential biological effects of three distinct commercially available functionalized PS nanoparticles (pristine, carboxylated, and aminated) with a size of about 50 nm on HUVECs, at a concentration of 100 μg/mL and after acute time-points exposures (20 min, 2, 12, and 24 h). The internalization of the nanoparticles was evaluated with different analytical methods including flow cytometry, confocal microscopy, and transmission electronic microscopy. Specifically, changes in cellular morphology (size and inner complexity), cytotoxicity, intracellular ROS production, and genotoxicity were evaluated for the different functionalized PS nanoparticles. This study provides new insights into the potential effects of differently functionalized PS nanoplastics on primary human endothelial cells, offering valuable information for assessing the health risks associated with PS-NPLs on the cardiovascular system.

2. Materials and methods

2.1. Polystyrene nanoplastics characterization

Three differently functionalized (pristine, carboxylated, and aminated) 50 nm commercialized polystyrene (PS) nanoplastics were purchased, both fluorescent-labeled (FL) and non-labeled (NL), from different companies. Namely, PS-Pristine 50 nm non-labeled (PS-P 50 NL; PP-008-10; nominal size 0.05–0.1 μm) and PS-Pristine 50 nm fluorescent-labeled (PS-P 50 FL; FP-00552-2; nominal size 0.04–0.09 μm; ex./em.: 460/480 nm) from Spherotech Inc. (Lake Forest, IL, USA); PS-Carboxylated 50 nm non-labeled (PS-C 50 NL; 15913-10; mean diameter 0.05 μm) and PS-Carboxylated 50 nm fluorescent-labeled (PS-C 50 FL; 16661-10; mean diameter 0.05 μm; ex./em.: 441/486 nm) from Polysciences Inc. (Warrington, PA, USA); PS-Aminated 50 nm non-labeled (PS-A 50 NL; 228PS50-AM-1; mean diameter 0.05 μm; ex./em.: 498/517 nm) and PS-Aminated 50 nm fluorescent-labeled (PS-C 50 FL; 228PS50-AMFC-1; mean diameter 0.05 μm) from Nanocs Inc. (New York City, NY, USA). All used polystyrene nanoplastics were supplied dispersed in water.

For characterization purposes, polystyrene nanoplastic dispersions were diluted in Milli-Q water and/or Endothelial Cell Growth Medium 2 (Promocell; Heidelberg, Germany). First, for dry state description by transmission electron microscopy (TEM), polystyrene particle working solutions were prepared on Milli-Q water at a concentration of 200 μg/mL. A cooper grid with carbon coverture was clamped and immersed into the working solution, placed on a filter paper-covered Petri dish, and allowed to evaporate overnight. The particles on the grid were placed on a single axis holder and examined using a transmission electron microscopy system operated at 120 kV JEOL JEM 1400 instrument (JEOL Ltd., Tokyo, Japan). Images were acquired using an Orius SC200D sensor from Gatan (Ametek, Inc. Berwyn, PA, USA) and analyzed for particle size distribution by measuring the Martin diameter using the ImageJ software 1.8.0_172. To investigate the potential influence of the culture medium on the colloidal structures in the suspension of the different PS nanoparticles, the behavior was studied using a Zetasizer®

Ultra device from Malvern Panalytical (Cambridge, UK). To such end, working solutions were prepared for each particle at a final concentration of 100 μg/mL, this time not only on Milli-Q water but also on EGM-2 culture medium. For sizing, 1 mL of each suspension was placed on a DTS0012 cuvette and measured with a collection angle of 174.8 whereas for Z-potential a slightly small volume was placed on a DTS1070 cuvette both cuvettes purchased on the same mentioned company. In both cases, three independent measurements were carried out.

2.2. Cell line and culture conditions

Human Umbilical Vein Endothelial Cells (HUVEC) were utilized as representative of the human endothelial barrier of the blood vessels. The cells were kindly provided by our collaborator Dr. Alejandro Portela (Universitat Internacional de Catalunya, Spain) and purchased from Promocell (Heidelberg, Germany) under the name of HUVEC single-donor C-12200. These endothelial cells are primary cells isolated from the endothelium of the umbilical cord vein and are frequently used for physiological and pharmacological investigations. Cells were cultured with Endothelial Cell Growth Medium 2 (EGM-2; C-22011) from Promocell (Heidelberg, Germany) in manually thin-layer collagen-coated flasks until passage 6 was reached to perform the different experiments. Cells were cultured at 37 °C in a humidified atmosphere with 5 % CO_2, and the medium was changed every two days. To prepare the collagen coating, rat collagen I (tail tendon) from Corning Inc. (New York City, NY, USA) was diluted to the desired concentration in 20 mM acetic acid to cover the flasks or plates at 5 μg/cm^2. After 1 h of incubation, the collagen was rinsed twice with 1× PBS to remove the excess acid.

2.3. Polystyrene nanoplastics treatments

To assess the potential toxicological impact of the different polystyrene nanoplastics, cells were subjected to nanoplastics diluted in EGM-2 medium at a concentration of 100 μg/mL for different exposure times. Typically, a brief exposure time of 2 h and an extended exposure time of 24 h were utilized. To maintain a consistent cell density between treatments with different exposure times, cells were examined at the exact moment by adjusting the application time of treatment. Predominantly, cells were seeded at a cell density of 26,300 cells/cm^2 and allowed to grow for 48 h in thin-layer collagen-coated wells (5 μg/cm^2). Subsequently, the medium was replaced with the desired treatment.

2.4. Cell viability assay

The viability of the HUVECs after exposure to the different non-labeled PS nanoplastics was determined using the Coulter method with a Beckman Coulter Z1-D cell counter from Beckman Coulter Inc. (Pasadena, CA, USA). Briefly, cells at passage 6 were seeded in 24 thin-layer collagen-coated well plates at a density of 26,300 cells/cm^2. After incubation for 48 h, cells were exposed to 100 μg/mL of the different non-labeled PS nanoplastics (PS-P 50 NL, PS-C 50 NL, and PS-A 50 NL) for 20 min, 2, 12, and 24 h to assess cell toxicity. Non-treated cells were used as a negative control. Following exposure, the cells were washed twice with 1× PBS to remove the treatments and allow the trypsinization with 100 μL/well trypsin-EDTA 1 % for 5 min at 37 °C. Trypsin was then inactivated with 200 μL/well of 5 % FBS diluted in 1× PBS. The detached cells were diluted 1:100 in ISOTON diluent and counted with the Beckman Coulter Z1-D cell counter. The obtained percentage values represent an average of the number of cells counted on each treatment, relative to the average of the number of cells counted in the corresponding untreated control. The experiment was performed three times and technical duplicates were analyzed for each treatment.

2.5. Cellular uptake (FACS, fluorescent activated cell sorter) and cell complexity (flow cytometry)

The internalization of polystyrene nanoplastics by HUVECs was first assessed by FACS. To such end, the fluorescent-labeled versions of the nanoparticles (PS-P 50 FL, PS-C 50 FL, PS-A 50 FL) were utilized. Cells at passage 6 were seeded in 24 thin-layer collagen-coated well-plates at a density of 26,300 cells/cm^2 and after 48 h of incubation were exposed to 100 μg/mL of PS-P 50 FL, PS-C 50 FL, and PS-A 50 FL for 20 min, 2, 12, and 24 h. A negative control was also included. After exposure, cells were washed twice with 1× PBS to remove the treatments and allow the trypsinization of the cells with 100 μL/well trypsin-EDTA 1 % for 5 min at 37 °C. Trypsin was inactivated with 200 μL/well of 5 % FBS diluted in 1× PBS. The *Via*-Probe™ Red Nucleic Acid Stain (BD Biosciences; Franklin Lake, NJ, USA) was added to a final concentration of 1:200 to stain live cells. The fluorescence of the cells was determined by the CytoFLEX FACS from Beckman Coulter (Pasadena, CA, USA). Nanoplastics internalization was analyzed with an excitation/emission spectra of 488/525 nm and *Via*-Probe™ with an excitation/emission of 638/660 nm wavelength, respectively. From this approach, the absolute number of cells that internalized polystyrene was determined, as well as the increase in fluorescence intensity relative to the control. This means that two parameters were determined i) the percentage of cells that have internalized labeled PS-NPLs, and ii) the amount of internalized labeled PS-NPLs per cell. For the second parameter, the respective kinetics curves over time were generated following a lognormal Gaussian fit, and internalization velocities were determined for the entire time range (absolute velocity; 0–24 h) and segments corresponding to the 0–2 h and 2–24 h intervals. The segmentation point was set at 2 h, considering that this is the time-point when almost all cells in the culture had internalized the different polystyrene nanoplastics. The absolute internalization velocity (iv_{abs}), was determined as follows: $iv_{abs} = \sqrt{(\Delta x/\Delta t)^2 + (\Delta y/\Delta t)^2}$. Similarly, internalization ratios were calculated between each segment velocity and the absolute internalization velocity. This analytical approach provided a nuanced understanding of the kinetics of polystyrene nanoplastics internalization over the specified time intervals.

Alternatively, forward and side scattering measurements from the flow cytometry were used to determine changes in the size and complexity of the cells, relative to the negative control. A total number of 10,000 cells were scored for all the treatments, and the data was analyzed using the Cytexpert software from Beckman Coulter (Pasadena, CA, USA). The experiment was carried out three times and technical duplicates were analyzed in each condition.

2.6. Cellular uptake assessment by confocal microscopy

To corroborate the exact localization of the fluorescent-labeled polystyrene nanoplastics (PS-P 50 FL, PS-C 50 FL, and PS-A 50 FL), laser confocal microscopy was utilized. Cells at passage 6 were seeded onto individual thin-layer collagen-coated μ-Dish 35 mm from Ibidi GmbH (Gräfelfing, Germany) at a density of 26,300 cells/cm^2. After 48 h, cells were exposed to 100 μg/mL PS nanoplastics for 24 h, with a non-treated negative control included. The culture media was removed, cells were washed twice with PBS 1×, and fresh media containing Hoechst 33342 (1:500) (ThermoFisher Scientific; Waltham, MA, USA) and Cellmask™ Deep Red plasma (1:500) (ThermoFisher Scientific; Waltham, MA, USA) to stain the nuclei and cell membranes, respectively, was added. Several images of each sample were taken using a Leica TCS SP5 (Leica Microsystems GmbH; Mannheim, Germany). PS nanoplastics were observed within the cells at an emission wavelength of 488 nm, whereas nuclei and cell membranes were visible at emission wavelengths of 405 and 633 nm, respectively. For each sample, several fields were randomly selected, and the images were processed using the Fiji extension of ImageJ software and Imaris Microscopy Image Analysis Software v. 9.6 from Oxford Instruments (Abingdon, England).

2.7. Cellular uptake assessment by transmission electron microscopy (TEM)

To complement the results obtained with flow cytometry and confocal microscopy, transmission electron microscopy (TEM) was also utilized. TEM allowed us to pinpoint the exact location of nanoplastics within the cells and identify the cellular structures that could potentially enclose them. To such end, HUVECs at passage 6 were cultured in 75 cm^2 thin-layer collagen-coated flasks at a density of 15.555 cells/cm^2. After 48 h cells were exposed to 100 μg/mL of non-labeled PS nanoplastics for 24 h; negative control with non-treated cells was included. Following the exposure, cells were washed twice with 1× PBS to remove the treatments and allow the trypsinization of the cells with 5 mL/flask trypsin-EDTA 1 % for 5 min at 37 °C. Subsequently, trypsin was inactivated with 10 mL/flask 2 % FBS diluted in 1× PBS, and cells were centrifuged for 6 min at 150*g* in 15 mL falcons' flasks. Pellets were resuspended in 2.5 % (v/v) glutaraldehyde (EM grade, Merck; Darmstadt, Germany) and 2 % (w/v) paraformaldehyde (EMS; Hatfield, PA, USA) in 0.1 M cacodylate buffer (Sigma-Aldrich, Steinheim, Germany), pH 7.4. Cell suspensions were transferred to 1.5 mL Eppendorf tubes (Eppendorf; Hamburg, Germany) and pelleted by centrifugation for 6 min at 150*g*. Samples were processed employing conventional techniques, as previously described (Annangi et al., 2015). Briefly, samples were post-fixed with osmium trioxide, dehydrated in acetone, embedded in Eponate 12™ resin (Ted Pella Inc.; Redding, CA, USA), and finally polymerized at 60 °C and cut with an ultramicrotome. Ultrathin sections were placed in copper grids, contrasted with uranyl acetate and Reynolds lead citrate solutions, and observed using a JEOL 1400 TEM (JEOL LTD; Tokyo, Japan) equipped with an ES1000W Erlangshen CCD camera (GATAN Inc.; Pleasanton, CA, USA).

2.8. Production of intracellular reactive oxygen species (ROS)

To assess intracellular ROS production, the dihydroethidium (DHE) method was performed. Cells at passage 6 were seeded in 24 thin-layer collagen-coated well plates at a density of 26,300 cells/cm^2, and after 48 h of incubation were exposed to 100 μg/mL of the different non-labeled PS nanoplastics for 20 min, 2, 12, and 24 h. A negative control (untreated cells) and a positive control (100 μM antimycin-A, treated for 45 min at 37 °C) were also included. After exposure, cells were washed twice with 1× PBS to remove the treatments and allow the trypsinization with 100 μL/well trypsin-EDTA 1 % for 5 min at 37 °C. DHE was added to 5 % FBS diluted in 1× PBS (trypsin inactivator) and 200 μL were added per well at a final concentration of 10 μM DHE. Cells in the DHE solution were transferred to 1.5 mL Eppendorf tubes and incubated for 30 min at 37 °C, protected from the light. The *Via*-Probe™ Red Nucleic Acid Stain (BD Biosciences; Franklin Lake, NJ, USA) was added to a final concentration of 1:200 to stain live cells. The fluorescence of the cells was measured using CytoFLEX LX flow cytometry from Beckman Coulter (Pasadena, CA, USA). The DHE signal was analyzed with an excitation/emission spectra of 561/585 nm and *Via*-Probe™ with an excitation/emission of 638/660 nm, respectively. A total of 10,000 cells were scored for all the treatments and the Cytexpert software from Beckman Coulter (Pasadena, CA, USA) was used to analyze the data. The experiment was conducted six times, with technical duplicates analyzed in each condition.

2.9. Genotoxicity induction detected by the comet assay

This study evaluated the levels of genotoxic damage, specifically DNA breaks, in HUVECs using the single-cell gel electrophoresis (SCGE) alkaline comet assay using GelBond® film (GBF) (Lonza Bioscience; Basel, Switzerland) as a support. For the experiment, cells at passage 6 were seeded in thin-layer collagen-coated 12 well plates at a density of 26,300 cells/cm^2 and after 48 h of incubation were exposed to 100 μg/mL of the different non-labeled PS nanoplastics for either 2 or 24 h. The experiment included a negative control (non-treated cells) and a positive control, with methyl methanesulphonate (200 μM for 30 min at 37 °C Sigma-Aldrich; St. Louis, MO, USA). After exposure, cells were washed twice with 1× PBS, detached with trypsin-EDTA 1 %, and trypsin-inactivated with 5 % FBS diluted in 1× PBS. Cells were centrifuged for 6 min at 150*g* at 4 °C in a microcentrifuge and resuspended with cold PBS to a final concentration of 1 × 10^6 cells/mL. Cell suspensions were mixed 1:10 with 0.75 % low melting point agarose at 37 °C, and a drop of 7 μL from each sample was placed on GBFs in triplicates. GBFs were left overnight in lysis buffer at 4 °C, washed in electrophoresis buffer for 5 min, and incubated in electrophoresis buffer for 35 min at 4 °C to allow DNA unwinding. After the incubation time, electrophoresis was performed at 20 V/300 mA at 4 °C for 20 min. GBFs were washed twice with cold PBS for 5 min and once with water for 1 min. Cells were fixed in absolute ethanol for 1 h and air-dried overnight at room temperature with proper light protection. Cells were stained with 1:10000 SYBER™ Gold (Invitrogen; Waltham, MA, USA) in TE buffer for 20 min at room temperature in continuous agitation. GBFs were washed in distilled H_2O and air-dried for one day before being mounted and visualized using an Olympus BX50 epifluorescence microscope (Olympus; Tokyo, Japan) at 20 X magnification. The DNA damage was analyzed with the Komet 5.5 image software (Kinetic Imaging Ltd.; Liverpool, UK) as the percentage of DNA in the tail. One hundred randomly selected cells were analyzed per sample. Two different samples were studied for each condition in each one of the two replicate experiments performed.

2.10. Statistical analysis

The data presented resulted from the average of different independent experiments (biological replicates), with the number of experiments stated in each section. Each experiment included at least two technical replicates for accuracy purposes. The data analyses were performed using GraphPad Prism 9 software (GraphPad Software Inc., CA, USA). The Shapiro-Wilk test was used as a normality test and the one-way ANOVA with Tukey's multiple comparison test for normal distributed data, or the Kruskal-Wallis test as a non-parametric test. Statistical significance was defined as $^{*}p \leq 0.05$, $^{**}p \leq 0.01$, and $^{***}p \leq 0.001$.

3. Results and discussion

3.1. Polystyrene nanoplastics characterization

The commercially obtained nanoplastics underwent further characterization through transmission electron microscopy (TEM) and dynamic light scattering (DLS) to determine key attributes including size, morphology, aggregation state, and surface charge when dispersed in both Milli-Q water and EGM-2 medium. As depicted in Fig. 1, TEM analysis revealed that, in line with the manufacturer's specifications, all particles were round-shaped with an approximate dry-state diameter of 50 nm. These size measurements exhibited some variability among particles, ranging from a minimum of 46.33 ± 11.18 nm (PS-P 50 FL) to a maximum of 76.45 ± 13.37 nm (PS-C 50 NL).

Upon investigating the hydrodynamic behavior of the nanoparticles in both Milli-Q water and EGM-2 medium, notable distinctions emerged. In general, Z-average sizes were larger in EGM-2 medium when compared to Milli-Q water. Furthermore, nanoparticles exhibited higher polydispersity indexes (PDI) in the EGM-2 medium, suggesting a tendency for particle aggregation when diluted in this culture medium containing various proteins. In terms of Z-potential, the obtained values exhibited fewer negative charges and showed fewer differences among the various functionalized nanoplastics when dispersed in media, compared to Milli-Q water. Similar differences in Z-potential and PDI values were obtained in a study comparing water and culture media dispersions with particles like we used (Paget et al., 2015). Such differences in Z-size average, polydispersity index, and Z-potential have

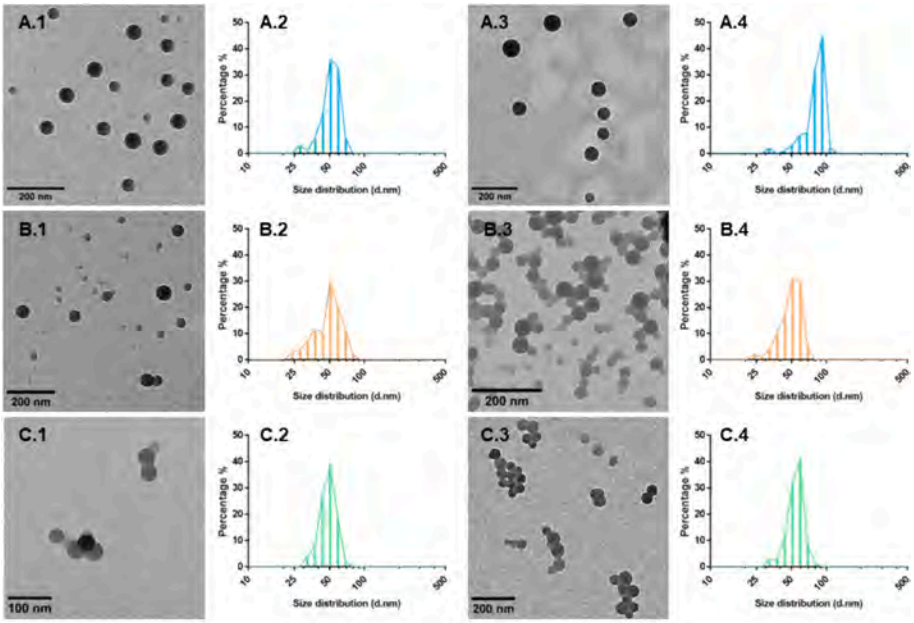

D

	MiliQ				EGM-2		
	TEM	Z-Average	PDI	Z-Pot	Z-Average	PDI	Z-Pot
PS-P 50 FL	46.33 ± 11.18	58.50 ± 1.07	0.01	-44.40 ± 0.83	130.00 ± 5.27	0.28	-5.58 ± 1.21
PS-P 50 NL	46.65 ± 9.00	94.00 ± 0.86	0.03	-44.90 ± 0.49	117.00 ± 2.64	0.26	-8.74 ± 2.22
PS-C 50 FL	48.23 ± 7.99	64.70 ± 0.55	0.03	-40.30 ± 1.99	691.00 ± 33.50	0.75	-9.34 ± 1.38
PS-C 50 NL	76.45 ± 13.37	60.10 ± 0.30	0.04	-43.20 ± 0.78	131.00 ± 1.17	0.06	-8.21 ± 1.14
PS-A 50 FL	45.31 ± 6.56	176.00 ± 0.88	0.19	+2.06 ± 0.89	129.00 ± 1.54	0.01	-4.69 ± 1.21
PS-A 50 NL	50.26 ± 5.57	213.00 ± 28.30	0.42	-21.80 ± 1.11	176.00 ± 12.30	0.34	-4.61 ± 0.95

Fig. 1. Polystyrene nanoplastics characterization. (A–C) shows TEM characterization in Milli-Q water for the different nanoparticles: (A) PS-Pristine, (B) PS-Carboxylated, (C) PS-Aminated. (A1–C1) TEM images for fluorescently labeled (FL) nanoparticles. (A2–C2) show the corresponding frequency histograms of the fluorescently labeled nanoparticle size distribution measured from the TEM images. (A3–C3) TEM images for the corresponding non-labeled (NL) counterparts of the different nanoparticles. (A4–C4) Frequency histograms of the non-labeled particle size distribution measured from TEM images. (D) TEM and DLS data for the different particles in Milli-Q water and EGM-2 media; sizes in d. nm and Z-potential in mV.

also been documented by several authors (Liu et al., 2020; Rampado et al., 2020; Vela et al., 2023) when nanoparticles interact with proteins and develop the denominated protein corona (PC). This PC surrounding the nanoparticles is known to reduce Z-potential values, thereby diminishing electrostatic repulsion, and promoting undesirable nanoparticle aggregation (as reflected by the higher PDI values).

A closer examination of the particles dispersed in media revealed that Z-average sizes did not exhibit significant differences among the different functionalizations, except for the fluorescently labeled carboxylated polystyrene version. This discrepancy can be attributed to its relatively high PDI value (0.75), indicating substantial nanoparticle aggregation/agglomeration in the media. Variations in nanoparticle aggregation/agglomeration result from surface properties which play a crucial role in determining the protein corona (Lundqvist et al., 2008). Although some differences in Z-potential could be expected between the different functionalizations, it is worth noting that these differences, which were noticeable in Milli-Q water, tended to diminish in the culture medium. The aminated version of the nanoparticles displayed a slightly less negative Z-potential when compared to the carboxylated and pristine particles, aligning with previous observations (Paget et al., 2015). Nevertheless, based on the physicochemical characteristics of the particle surface and the findings of other researchers, more substantial Z-potential differences were expected among the different surface-functionalized polystyrenes (Banerjee et al., 2021). Lastly, negligible disparities were observed between the non-labeled nanoparticles and their fluorescently labeled counterparts, except for PS-C 50 FL, as previously mentioned.

3.2. Toxicity of the evaluated PS-NPLs

To compare the cytotoxic potential of the three differently functionalized polystyrene nanoparticles (pristine, carboxylated, and aminated), HUVECs were exposed to a concentration of 100 μg/mL in a time interval ranging from 20 min to 24 h. This concentration was chosen according to the lack of toxicity shown by PS-NPLs in previous studies using different cell lines (Annangi et al., 2023; Vela et al., 2023; Tavakolpournegari et al., 2023). As illustrated in Fig. 2, all particle types induced a significant reduction in cell viability, even at the shortest exposure time of 20 min, showing a special sensitivity of HUVECs to PS-NPLs. However, if we apply the criteria outlined in ISO 10993-5:2009 (E), which defines cytotoxicity as a reduction in cell viability exceeding 30 %, it can be concluded that only aminated polystyrene exhibited cytotoxicity towards HUVECs at 100 μg/mL, with a 37.95 % reduction in viability observed at the 12 h treatment. The most substantial reductions in viability for pristine and carboxylated PS nanoparticles reached 25.20 % at 24 h and 20.44 % at 12 h, respectively.

The cytotoxic potential of aminated PS was previously reported in HUVECs (Fu et al., 2022). In their study, the authors described concentration- and time-dependent cytotoxicity for aminated PS-treated cells after 12 and 24 h of exposure. In their research, cell survival rates fell below 30 % with a dose of 20 μg/mL, providing clear evidence of cytotoxic effects. The heightened cytotoxicity of aminated PS may stem from its increased positive charge, facilitating an enhanced interaction with negatively charged membranes. This interaction could potentially lead to membrane disruption and subsequent cellular damage, as hypothesized by Ruenraroengsak et al. (2012) and Fu et al.

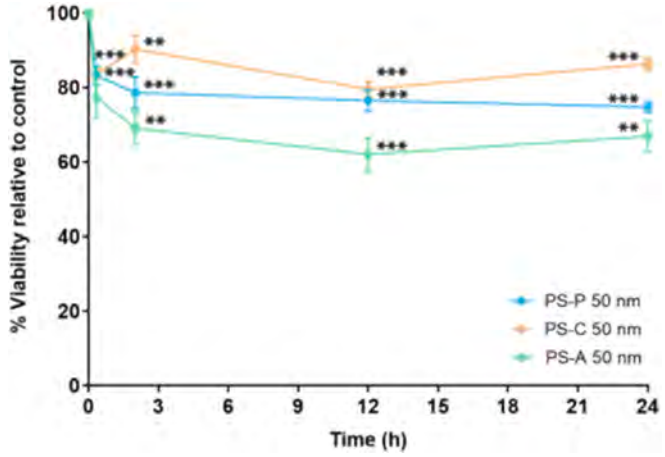

Fig. 2. Relative cell viability of HUVECS after exposure to the different PS nanoplastics at 100 μg/mL for 20 min, 2, 12, and 24 h exposure times. Data is represented as the percentage of living cells relative to the untreated control ± SEM. One-way ANOVA with Dunnett's post-test (normal distributed data) and Kruskal-Wallis's test (non-parametric test) were used for the statistical analysis. Statistical significance was indicated in the graph as $^{**}p < 0.01$ and $^{***}p < 0.001$.

(2022).

Differential cytotoxicity among pristine, carboxylated, and aminated PS was observed in other primary cells, including primary human alveolar type 2 epithelial cells and primary human alveolar macrophages (Ruenraroengsak and Tetley, 2015). This would indicate a special sensitivity of primary cells in comparison with established cell lines.

3.3. Assessing cell internalization of PSNPLs by different analytical methods

To correctly understand the toxicological profile of any MNPLs, it is essential to know their ability to internalize in the used cell line. In this study, cellular internalization of the PS nanoparticles was determined by different analytical methods, including flow cytometry, confocal microscopy, and transmission electron microscopy (TEM). This multimodal approach was followed since the different methods can complement each other, overcoming the individual limitations of each technique and providing a more robust result.

3.3.1. Cellular internalization by FACS

To investigate the internalization dynamics of the different PS nanoparticles FACS analyses were performed after treating the cells with the fluorescent-labeled counterparts of the particles at different time points (20 min, 2, 12, and 24 h). As depicted in Fig. 3A, HUVEC cells exhibited a rapid internalization dynamic for all types of nanoplastics. Our findings indicate that for both surface-modified carboxylated and aminated polystyrene nanoparticles the rate of positive cells internalizing nanoplastic was 95–100 % within just 20 min, while pristine nanoplastics required a slightly longer exposure time, with 40.94 % internalization at 20 min and 88.82 % at 2 h. Although some studies have reported data on the internalization of PS-C (Ho et al., 2018) and PS-A (Wei et al., 2022) in HUVECs, they used different methodological approaches, and no comparisons regarding the role of functionalization were established. Thus, our approach is a novelty in this type of cell. However, studies investigating the implications of surface functionalization on PS-NPLs internalization have been done on human hepatocellular carcinoma (HepG2) cells (He et al., 2020; Banerjee et al., 2022) showing a higher internalization of functionalized 50 nm PS-NPLs regarding the pristine version.

When analyzing the cell internalization kinetics (Fig. 3B), relying on absolute FITC fluorescence arbitrary values, we could infer that carboxylated PS exhibited the most substantial internalization by HUVECs after 24 h exposure (855.67 FITC folds related control). Following this, pristine PS was internalized to a lesser extent (96.69 FITC folds *vs* control at 24 h), while aminated PS demonstrated the lowest degree of internalization (41.48 FITC folds *vs* control at 24 h). It is important to notice that the differences in fluorescence can be misleading because they may arise due to variations in the fluorophores employed by the different companies in the production of the labeled nanoparticles. Therefore, we used a multi-parameter approach to minimize such uncertainty, incorporating TEM imaging analysis and flow cytometry size/complexity comparisons, as further discussed in detail in this manuscript. These complementary analyses reinforced and aligned with the trends observed in the FACS data, providing a more comprehensive understanding of nanoparticle internalization.

The internalization dynamics fitted to a lognormal Gaussian model in the three different treatment approaches (as can be observed in Supplementary Fig. S1). This modeling allowed us to establish differences in the internalization velocity of the different functionalized nanoplastics over time. At short-term treatments (0–2 h), aminated PS exhibited the fastest internalization velocity (5.13 folds *vs* its absolute *iv*), followed by carboxylated PS (3.43 folds when compared to its absolute *iv*) and, finally, the non-functionalized one (1.28 folds *vs* absolute *iv*). These trends, observed at short exposure times, seem to have an impact on the second part of the curve, regardless of the absolute quantity of internalized plastics. We can observe that after 2 h for pristine PS, the decrease in the velocity reaches up to 0.97 of the mean velocity, while it

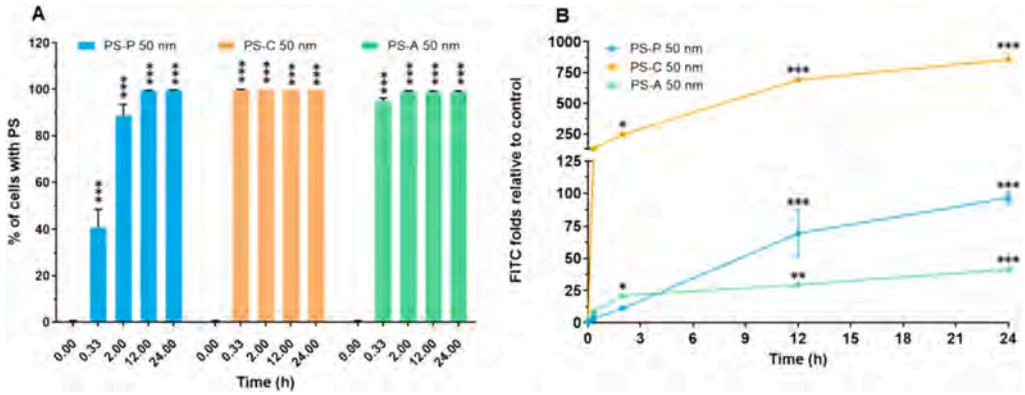

Fig. 3. (A) Quantification by FACS of the percentage of cells that have internalized the different PS nanoplastics at 100 μg/mL for 20 min, 2, 12, and 24 h exposure times. (B) Internalization kinetics (measured as FITC folds relative to control) of different PS nanoplastics at 100 μg/mL for 20 min, 2, 12, and 24 h exposure times in HUVEC. Data is represented as mean ± SEM. One-way ANOVA with Dunnett's post-test (normal distributed data) and Kruskal-Wallis's test (non-parametric test) were used for the statistical analysis. Statistical significance was indicated in the graph as $^{*}p < 0.05$, $^{**}p < 0.01$ and $^{***}p < 0.001$.

reaches 0.78 for carboxylated, and 0.70 for aminated. The faster uptake of aminated PS compared to carboxylated PS that we described at short-time periods (0–2 h) was also noted in a study involving human alveolar cells (Roshanzadeh et al., 2020). That may be attributed to the presence of positive substitution groups (—NH_2) on aminated particle surfaces, which can bind to the anionic headgroups of phospholipids or other negatively charged molecules on membrane proteins, facilitating the internalization, as larger electrostatic interactions tend to result in more effective cellular uptake (Roshanzadeh et al., 2020). Additionally, differences in internalization pathways could play a role, as particle charge is known to influence this process. For instance, anionic particles primarily undergo internalization through clathrin/caveolae-independent endocytosis, while cationic particles are often taken up *via* micropinocytosis (Foroozandeh and Aziz, 2018). However, studies aiming to elucidate the internalization pathways of nanoparticles in HUVECs have indicated that clathrin- and caveolae-based cellular uptake plays a significant role in the internalization of particles up to 180 nm in size (Ho et al., 2018). These findings underscore the complexity surrounding nanoparticle endocytosis mechanisms and emphasize the need for further research to clarify how nanoparticle surface functionalization affects the internalization pathways in HUVECs. It is important to note that our results, related to the absolute measurement of cellular uptake, agree with those reported in the literature.

3.3.2. Cellular internalization by confocal microscopy

By using confocal microscopy, we were able to visually ascertain the location of the nanoparticles inside the cells and distinguish if they were located within the cells or externally attached to the plasma membrane. The z-stacks images obtained *via* confocal microscopy (Fig. 4) demonstrate that after 24-h of treatment, the nanoparticles were distributed throughout the entire cytoplasm, rather than being affixed/adhered to the cell membrane. Additionally, some particles were observed close to the nucleus, suggesting potential interactions with this cellular compartment and/or its genetic material (Fig. 4A). In a general way, it is evident that after 24 h of exposure all treated cells have a big portion of the cytoplasm covered with the fluorescence emitted by nanoplastics (Fig. 4A–C), which is coherent with the previously described FACS data.

3.3.3. Cellular internalization by TEM

Transmission electron microscopy (TEM) was used to visualize and confirm the presence of unlabeled PS-NPLs nanoplastics in cell ultrastructure. The Fig. 5A–B illustrates the remarkable accumulation of nanoparticles in vesicles within HUVECs after 24 h exposure to the concentration of 100 μg/mL, both using pristine and carboxylated PS-NPLs. These findings are comparatively congruent with the distribution of the fluorescence observed in Fig. 4, where the amount of signal was rather concentrated on focused spots distributed over the cell structure (Fig. 4A–C). Therefore, it is relevant to note the different distribution of the functionalized nanoparticles inside the cells. First, and as depicted in Fig. 5A.1–2, pristine PS nanoparticles were found enclosed inside vesicles that can have up to 5 μm diameter, covering most of the cell cytoplasm. These vesicles exhibited well-defined membranes and an irregular pattern of electro-dense regions inside, which precluded the direct measurement or identification of individual nanoparticles. Additionally, smaller vesicles of approximately 1 μm diameter were also observed (see Supplementary Information, Fig. S2). Interestingly, these smaller vesicles were filled with round-shaped structures measuring 50–60 nm in diameter, consistent with the expected size of the used nanoplastics. Both types of vesicles, observed in the pristine treatments, were found in varying proportions among individual cells. Notably, the presence of these vesicles within the cytoplasm resulted in the reorganization of intracellular organelles and the nucleus, as described in Caco-2 cells (Cortés et al., 2019). Similar structures resembling the smaller vesicles (around 1 μm in diameter) were previously reported in HUVECs following treatment with 100 nm PS nanoplastics (Lu et al., 2022), as well as in other cells, such as Caco-2, after exposure to 50 nm

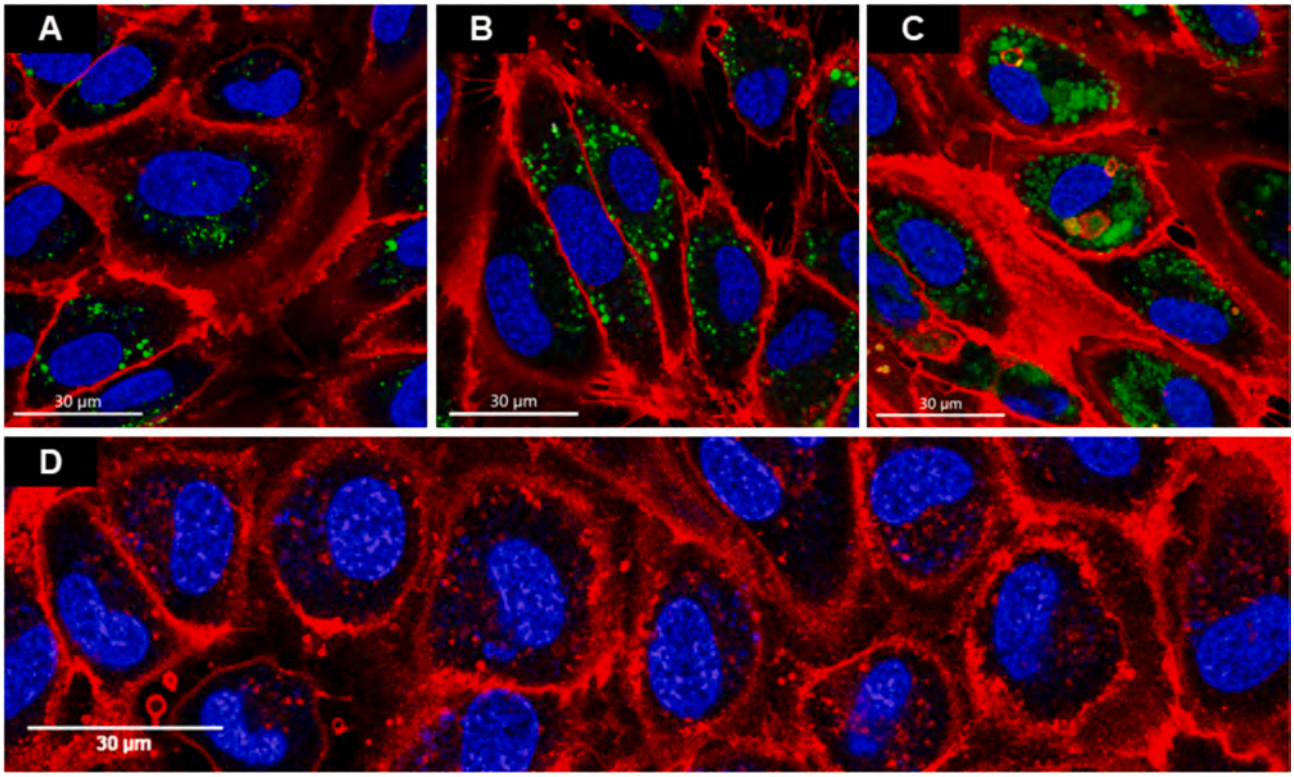

Fig. 4. Confocal images of polystyrene nanoplastics internalization by HUVECs exposed to 100 μg/mL for 24 h: (A) PS-Pristine, (B) PS-Carboxylated, (C) PS-Aminated, (D) Negative control. Different polystyrene nanoplastics (green), nuclei (blue), and cell membranes (red) were stained with Yellow-green core fluorophore, Hoechst 33342, and CellMask™, respectively.

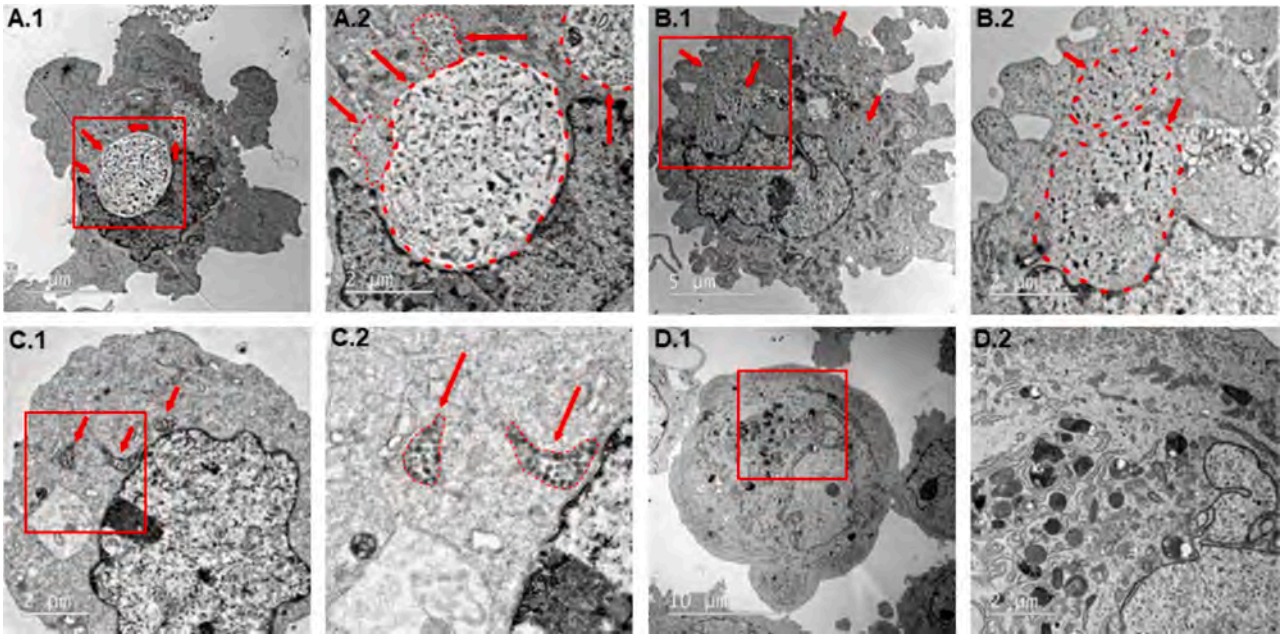

Fig. 5. TEM images of different PS nanoplastics at 100 μg/mL for 24 h exposure time in HUVECs. (A.1–A.2) Pristine PS treatment; vesicles up to 5 μm diameter can be found in the cytoplasm of the cells. Highlight the presence of different textures/patterns among the different vesicles. (B.1–B.2) In the cells treated with Carboxylated PS, 5 μm diameter vesicles can be observed with the presence of electrodense undefined structures inside. (C.1–C.2) Aminated PS treatment; 500–700 nm vesicles can be found filled with rounded shape structures of around 90 nm. (D.1–D.2) Shows the negative control with the absence of any vesicles that can suggest the presence of PS nanoplastics. Solid red squares indicate a zoom-in region; vesicles are pointed with red arrows and red dashed lines highlight its margins in all the pictures.

PS (Domenech et al., 2021). In cells treated with carboxylated polystyrene (Fig. 5B.1–2), vesicles exhibited similar characteristics, such as well-defined membranes, diameters of up to 5 μm, and an irregular electron-dense inner pattern, were also observed. The reorganization of the organelles and nucleus inside the cell was also present due to the size of the vesicles that covered a major part of the cytoplasm. Conversely, in the case of PS-aminated treatment, the number of vesicles was dramatically reduced, but in all cases, vesicles containing electron-dense dots measuring around 90 nm in diameter were found (Fig. 5C1–2). These vesicles were smaller than those beforehand described treatments, and the sizes were usually on the submicrometric scale, ranging predominantly from 500 to 700 nm in diameter, displaying irregularity in shapes as a common characteristic. PS-NPLs were detected confined within these structures which look like those previously described as autophagosomes following treatment with 100 nm pristine PS-NPLs (Lu et al., 2022). Additionally, non-canonical multilamellar bodies were found with a higher prevalence in these aminated PS-treated cells (Fig. S3). The only mention in the literature, resembling the structures we observed is a recently described putative phosphate-sensing organelle in *Drosophila melanogaster* midgut cells (Xu et al., 2023). Importantly, none of the structures described above were found in any of the negative controls (Fig. 5D1–2), after analyzing a substantial number of cells, indicating that the formation of these vesicles was caused by the treatments.

Collectively, our findings, supported by flow cytometry data, confocal microscopy imaging, and TEM images, consistently demonstrate a rapid and substantial internalization of PS nanoparticles by HUVECs under our experimental conditions for both pristine and carboxylated treatments. The limited number of vesicles observed in TEM images after aminated PS treatment is in line with the flow cytometry and confocal data. For the last technique, we can easily see differential intensities with more concentrated photons in the case of PS and PS-C and widely dispersed for PS-A, which can correlate with the presence/absence of vesicles. This could be attributed to the fact that once the aminated nanoparticles were inside the cell, these dispersed individually throughout the cytoplasm instead of being encapsulated within vesicles. It is important to note that the low atomic number of polymers in that nanoplastic could cause them to weakly scatter electrons that may result in a poor TEM contrast to observe individual nanoparticles (Sawyer et al., 2008). Something similar could happen if each vesicle is loaded with a few particles. Another additional explanation could relate to the different internalization pathways, resulting in the formation of various vesicle/structure types within cells, which may vary in their TEM visibility due to their inherent properties.

3.4. Size and inner complexity as assessed by flow cytometry

Flow cytometry forward scattered light (FSC) provides basic morphological information, such as relative cell size. Additionally, light scattered at a 90° angle to the incident beam (SSC) arises from refracted and reflected light and serves as an indicator of the internal cell granularity/complexity within the cell cytoplasm (Jaroszeski and Radcliff, 1999). Based on this principle, known as Mie scattering, forward- and side-scattered light offered valuable data regarding alterations in cell size and inner complexity resulting from the applied treatments.

In our study, statistically significant changes in cell size were found in treatments lasting for 12 and 24 h with both pristine and carboxylated PS-NPLs, displaying a time-dependent pattern (Fig. 6A). The increase in cell size was more pronounced at 24 h for carboxylated PS-NPLs (30 % increase relative to the negative control) compared to pristine forms (20 % increase relative to the negative control). No significant alterations in cell size were observed after treatment with aminated PS at any of the evaluated time points. Concerning cell complexity, a parameter previously utilized in our research group to detect cellular uptake of different nanomaterials (Vila et al., 2017; Villacorta et al., 2022), a pattern like for cell size was noted (Fig. 6B). This parameter exhibited its most substantial increase at 24 h of exposure with carboxylated PS-NPLs (56 % increase compared to the negative control). Treatment with aminated nanoparticles also resulted in a slight, yet statistically significant, increase in cell complexity at 24 h (20 % increase compared to the negative control). Similar increases in cell complexity were described in HUVECs following 3 h treatments with 80 nm AuNPs, although no

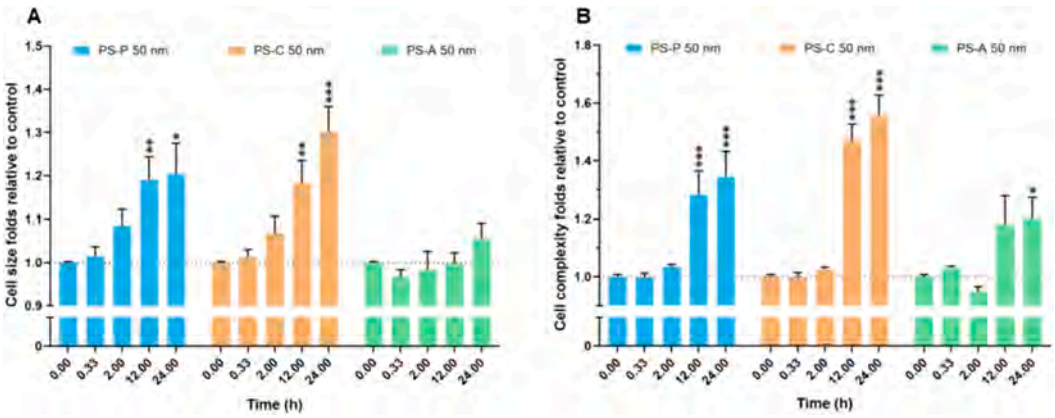

Fig. 6. Relative increment in cell size (A) and cell complexity (B) at exposure to different PS -NPLs at 100 μg/mL for 20 min, 2, 12, and 24 h, respectively. Data is represented as mean ± SEM. One-way ANOVA with Dunnett's post-test (normal distributed data) and Kruskal-Wallis's test (non-parametric test) were used for the statistical analysis. Statistical significance was indicated in the graph as $*p < 0.05$, $**p < 0.01$ and $***p < 0.001$.

changes in cell size were determined between exposed and unexposed cells (Klingberg et al., 2015). In human alveolar A549 cells, modest increases in both size and complexity were observed when exposed to carboxylated and aminated PS-NPLs (20 and 200 nm) (Kihara et al., 2021).

The obtained results suggest that pristine and carboxylated nanoparticles induce time-dependent changes in cell size and inner complexity, with carboxylated treatment exhibiting a more pronounced effect, which is coherent with the other approaches used on this study. Conversely, aminated PS treatment led to only slight increases in cell complexity at 24 h of treatment, which correlated with the limited number of vesicles observed in the TEM images. The absence or limited changes in cell size and complexity following PS-A treatment, in conjunction with the TEM and FACS results, highlight potential differences in internalization and particle disposition within the cells for aminated nanoparticles compared to pristine and carboxylated. This underscores the role of nanoparticle surface properties in cellular uptake and the potential subsequent effects. Further research should be carried out to explore the impact of size increases induced by pristine and carboxylated PS nanoplastics in three-dimensional models like tissue engineering blood vessels (Son et al., 2021).

3.5. Intracellular ROS production

Once demonstrated the role of functionalization in the internalization ability of PS-NPLs, their potential effects on cell functionality should be known. Among the different hazards associated with nanoparticle exposures, the induction of intracellular reactive oxygen species (iROS) stands out (Yu et al., 2020). Thus, iROS increases have been widely reported in different *in vivo* and *in vitro* studies after exposures to MNPLs. These investigations have been performed in different aquatic organisms, such as zebrafish (Sökmen et al., 2020) and *Drosophila* (Alaraby et al., 2023), and in cell lines including hematopoietic human cell lines (Rubio et al., 2020b; Vela et al., 2023), and notably, HUVECs. The studies of iROS imbalance in HUVECs are of major concern, as excessive ROS production in endothelial cells has been linked to cellular apoptosis and inflammatory mechanisms that play a pivotal role in atherosclerosis development, the leading cause of coronary heart disease (Li et al., 2017). Notably, a study performed in HUVECs described how ROS production triggered by amorphous SiO_2 nanoparticles played a central role in the assembly of the NLRP3 inflammasome and upregulation of HMGB1, subsequently activating MyD88 and NF-κB signaling pathways, leading to cellular inflammation (Liu et al., 2021).

In our study, we pursued to understand the influence of the time exposure, ranging from 20 min to 24 h in the levels of iROS. Investigating both short and long treatment times is crucial when studying iROS since the production and maintenance of these species within the cell is a dynamic process. Focusing solely on short periods may underestimate iROS production, as it does not provide sufficient time for enhanced production by the treatment; however, studying only longer durations may underestimate its induction due to the elimination of iROS by cellular protective mechanisms.

As depicted in Fig. 7, all three different treatments led to a significant increase in intracellular ROS production in all studied time points. While the differences between the time points were minimal, the smallest increases were consistently observed at the 12 h time point, with the most substantial increases occurring at 2 and 24 h time points, compared to negative controls. The heightened production of iROS in HUVECs following nanopolystyrene treatment was expected, as it was previously reported in studies such as after 30 nm carboxylated PS-NPLs exposure (Wei et al., 2022) and after 50 nm pristine and aminated PS-NPLs (Fu et al., 2022).

Interestingly, among the different functionalization of PS-NPLs, the lowest increases in iROS were consistently associated with the pristine treatment (*e.g.*, 21 % increase *vs* negative control at 24 h), while both carboxylated and aminated treatments exhibited very similar and higher values (*e.g.*, 30 % increase *vs* negative control at 24 h). This surface-dependent effect revealed in our study diverged from those findings

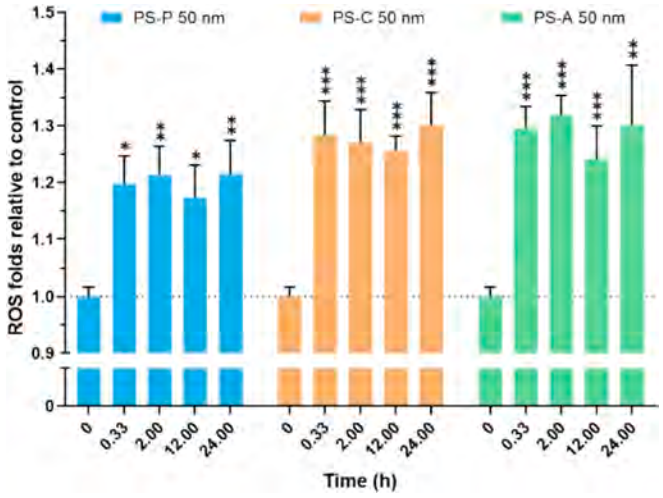

Fig. 7. Relative iROS production in HUVEC treated with different PS nanoplastics at 100 μg/mL for 20 min, 2, 12, and 24 h, as detected with DHE assay. Data is represented as mean ± SEM. One-way ANOVA with Dunnett's post-test was used for the statistical analysis. Statistical significance was indicated in the graph as $*p < 0.05$, $**p < 0.01$, and $***p < 0.001$.

reporting similar results for both 50 nm pristine and aminated nanoparticles (Fu et al., 2022). However, a major iROS production after aminated treatment, compared to pristine, was reported in human alveolar type II A549 cells (Halimu et al., 2022).

The enhanced iROS production following the aminated treatment could be explained by its stronger ability to interact with mitochondria, one of the main producers of intracellular ROS (Tirichen et al., 2021). Indeed, a major dysregulation of mitochondrial dynamics, replication, and function-related gene expression was observed after aminated treatment when compared to pristine PS-NPLs (Fu et al., 2022). As for the carboxylated nanoparticle, its capacity to increase ROS production could be explained by its major internalization compared to the pristine particle, as indicated by the major observed increases in cell size and complexity previously described.

3.6. Genotoxicity detection by the comet assay

Confocal microscopy and TEM images revealed a close spatial relationship between the nanoparticle vesicles and the nucleus of the cells, especially for the pristine and carboxylated PS-NPLs treatments. This interaction of the vesicles with the nucleus, which even reshaped the nuclear morphology, together with the increment of iROS, raised our concerns about the potential genotoxic effects of the evaluated PS-NPLs. In general, scarce studies have been undertaken to date to evaluate the genotoxic potential of such particles in human cells, with no prior studies recorded for HUVECs. Thus, considering the importance of genotoxicity as a surrogate biomarker of carcinogenesis (Shi et al., 2022), the alkaline comet assay was conducted to examine the induction of genotoxic damage by the differently functionalized polystyrene nanoplastics. The comet assay detects mainly DNA strand breaks, and it has been described as a reliable tool for detecting the genotoxic potential of metal-oxide nanoparticles (García-Rodríguez et al., 2019). Our results show that all PS-NPLs induce significant increases in DNA damage, after short exposures lasting for 2 h when the percentage of DNA in the tail is used as a biomarker (Fig. 8A). At these exposure times, pristine polystyrene induced the highest level of genotoxicity (57 % higher than the negative control), followed by aminated PS (39 % higher than the negative control). Carboxylated PS nanoparticles exhibited the lowest genotoxic effect, with a 24 % increase regarding the negative control.

To better understand the effects measured by the comet assay, a set of representative figures of the different treatments is presented in Fig. S4.

When exposures were extended to 24 h (Fig. 8B), the genotoxic effects appeared to diminish for both the pristine (28 % DNA in the tail *vs* control) and carboxylated forms (8 % DNA in the tail *vs* control), while remaining consistent for the aminated nanoparticle treatment. In this case, the aminated treatment reached the highest percentage of DNA in the tail when compared to the other treatments (39 % increase *vs* negative control). This general reduction in genotoxicity over time could be attributed to the concurrent repair of DNA lesions within the cells, as DNA repair mechanisms work to correct damage caused by genotoxic agents (Roursgaard et al., 2022).

It is noteworthy to compare these results with other studies utilizing the comet assay, which have reported little to no genotoxic effects of 50 nm PS nanoparticles in human cell lines, such as intestinal cells or white blood cells (Ballesteros et al., 2020; Domenech et al., 2020). Contrary, genotoxic effects for pristine, carboxylated, and aminated 80 nm PS-NPLs were reported in A549 cells at exposures lasting for 24 h but using the micronucleus assay instead of the comet assay (Shi et al., 2022). In such a study, the highest genotoxic effects were observed with aminated nanoparticles, followed by carboxylated, and pristine nanoparticles. The differences in genotoxicity reported in our study may be attributed to the differences in nanoparticle surface properties, although the cell type used can explain the differences with other studies. Nevertheless, our results are of high relevance since they have been obtained with human-derived primary cells, which are known to provide more physiologically relevant results than other immortalized and cancerous cell lines (Richter et al., 2021).

4. Conclusions

The human umbilical vein endothelial cells (HUVEC) utilized in this study are a good cell model for determining the kinetic cell uptake of PS-NPLs. These cells, as representative of the human endothelial barrier of the blood vessels, are primary cells isolated from the endothelium of the umbilical cord vein, which highlights the value of the obtained results. This model has confirmed that the functionalization of the PS-NPLs surface modulates their ability to internalize, pristine showing the slowest internalization. Moreover, it must be emphasized that even considering the lesser overall internalization, the main biological effects were found when cells were treated with aminated substituted nano polystyrene. This can give a different mindset related to what could or may be considered an effective dose more than a concentration-related treatment. The slow uptake of aminated polymers is associated with the relative increment in size and complexity of the cells exposed to the aminated type. Interestingly, all together show us that a slow

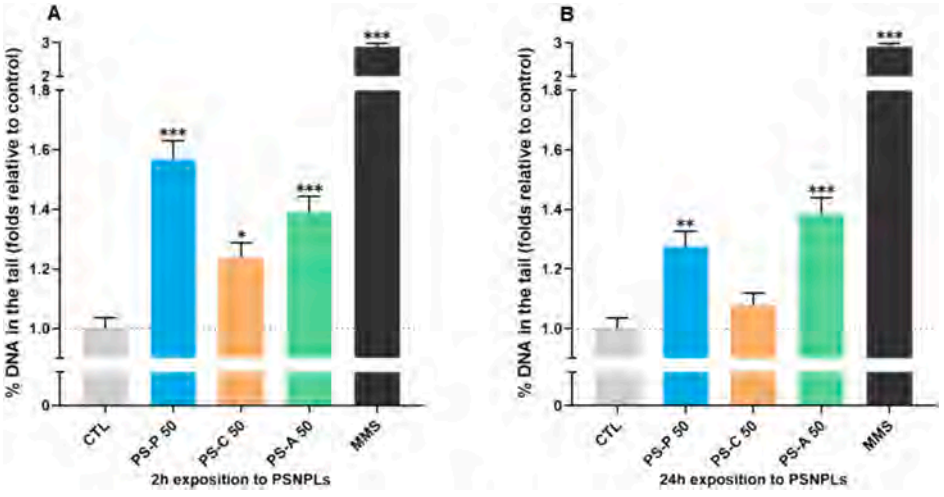

Fig. 8. Genotoxic damage detection in HUVEC by using the comet assay after exposures lasting for 2 h (A) and 24 h (B) to different PS-NPLs at 100 μg/mL. The concentration of 200 μM MMS was used as a positive control. Data is represented as mean ± SEM. The Kruskal-Wallis's test was used for statistical analysis. Statistical significance was indicated in the graph as $*p < 0.05$, $**p < 0.01$, and $***p < 0.001$.

internalization kinetics does not affect the ability of the aminated PS-NPLs to induce damage in the exposed cells, as determined by the ability to increase the intracellular ROS levels as well as their genotoxic potential, measured by the ability to induce DNA breaks. These effects of the surface characteristics should be considered when new true-to-life MNPLs, resulting from the degradation of plastic goods, are evaluated. Thus, determinations of the surface characteristics should be included in studies aiming to determine the hazardous effects of MNPLs.

Given that endothelial cells (such as HUVECs) constitute the main component of the human endothelial barrier within blood vessels, further investigation is warranted to comprehend the effects of variously functionalized and sized polystyrene (PS) nanoparticles (and MNPLs in general) on the endothelial barrier integrity. Notably, a phenomenon known as nanoparticle-induced endothelial leakiness (NanoEL) has already been documented for gold nanoparticles ranging from 10 to 30 nm (Setyawati et al., 2017), which must be explored using NPLs.

CRediT authorship contribution statement

Joan Martín-Pérez: Formal analysis, Investigation, Methodology, Writing – original draft. **Aliro Villacorta:** Investigation, Methodology. **Gooya Banaei:** Investigation, Methodology. **Michelle Morataya-Reyes:** Investigation, Methodology. **Alireza Tavakolpournegari:** Investigation, Methodology. **Ricard Marcos:** Conceptualization, Writing – review & editing. **Alba Hernández:** Writing – review & editing. **Alba García-Rodriguez:** Conceptualization, Writing – original draft, Writing – review & editing.

Declaration of competing interest

The authors declare that they have no known competing financial interests or personal relationships that could have appeared to influence the work reported in this paper.

Data availability

Data will be made available on request.

Acknowledgments

JM, MMR, and AT hold Ph.D. fellowships from the Generalitat de Catalunya. AV was supported by a Ph.D. fellowship from the National Agency for Research and Development (ANID), CONICYT PFCHA/DOCTORADO BECAS CHILE/2020-72210237. AGR received funding from the postdoctoral fellowship program Beatriu de Pinós (AGAUR, Goverment of Catalonia and Horizon 2020). AH was granted an ICREA ACADEMIA award.

The PlasticHeal project has received funding from the European Union's Horizon 2020 research and innovation programme under grant agreement No 965196. This study was supported by the Spanish Ministry of Science and Innovation (PID2020-116789RB-C43) and the Generalitat de Catalunya (2021-SGR-00731).

Appendix A. Supplementary data

Supplementary data to this article can be found online at https://doi.org/10.1016/j.scitotenv.2024.173236.

References

Alaraby, M., Villacorta, A., Abass, D., Hernández, A., Marcos, R., 2023. The hazardous impact of true-to-life PET nanoplastics in *Drosophila*. Sci. Total Environ. 863, 160954 https://doi.org/10.1016/j.scitotenv.2022.160954.

Alimi, O.S., Claveau-Mallet, D., Kurusu, R.S., Lapointe, M., Bayen, S., Tufenkji, N., 2022. Weathering pathways and protocols for environmentally relevant microplastics and nanoplastics: what are we missing? J. Hazard. Mater. 423 (Pt A), 126955 https://doi.org/10.1016/j.jhazmat.2021.126955.

Annangi, B., Bach, J., Vales, G., Rubio, L., Marcos, R., Hernández, A., 2015. Long-term exposures to low doses of cobalt nanoparticles induce cell transformation enhanced by oxidative damage. Nanotoxicology 9 (2), 138–147. https://doi.org/10.3109/17435390.2014.900582.

Annangi, B., Villacorta, A., López-Mesas, M., Fuentes-Cebrian, V., Marcos, R., Hernández, A., 2023. Hazard assessment of polystyrene nanoplastics in primary human nasal epithelial cells, focusing on the autophagic effects. Biomolecules 13 (2), 220. https://doi.org/10.3390/biom13020220.

Bajt, O., 2021. From plastics to microplastics and organisms. FEBS Open Bio 11 (4), 954–966. https://doi.org/10.1002/2211-5463.13120.

Ballesteros, S., Domenech, J., Barguilla, I., Cortés, C., Marcos, R., Hernández, A., 2020. Genotoxic and immunomodulatory effects in human white blood cells after *ex vivo* exposure to polystyrene nanoplastics. Environ. Sci. Nano 7, 3431–3446. https://doi.org/10.1039/D0EN00748J.

Banerjee, A., Billey, L.O., Shelver, W.L., 2021. Uptake and toxicity of polystyrene micro/nanoplastics in gastric cells: effects of particle size and surface functionalization. PLoS One 16 (12), e0260803. https://doi.org/10.1371/journal.pone.0260803.

Banerjee, A., Billey, L.O., McGarvey, A.M., Shelver, W.L., 2022. Effects of polystyrene micro/nanoplastics on liver cells based on particle size, surface functionalization, concentration, and exposure period. Sci. Total Environ. 836, 155621 https://doi.org/10.1016/j.scitotenv.2022.155621.

Cao, Y., Gong, Y., Liu, L., Zhou, Y., Fang, X., Zhang, C., Li, Y., Li, J., 2017. The use of human umbilical vein endothelial cells (HUVECs) as an *in vitro* model to assess the toxicity of nanoparticles to endothelium: a review. J. Appl. Toxicol. 37 (12), 1359–1369. https://doi.org/10.1002/jat.3470.

Cortés, C., Domenech, J., Salazar, M., Pastor, S., Marcos, R., Hernández, A., 2019. Nanoplastics as a potential environmental health factor: effects of polystyrene nanoparticles on human intestinal epithelial Caco-2 cells. Environ. Sci. Nano 7 (1), 272–285. https://doi.org/10.1039/C9EN00523D.

Domenech, J., Marcos, R., 2021. Pathways of human exposure to microplastics, and estimation of the total burden. Curr. Opin. Food Sci. 39, 144–151. https://doi.org/10.1016/j.cofs.2021.01.004.

Domenech, J., Hernández, A., Rubio, L., Marcos, R., Cortés, C., 2020. Interactions of polystyrene nanoplastics with *in vitro* models of the human intestinal barrier. Arch. Toxicol. 94 (9), 2997–3012. https://doi.org/10.1007/s00204-020-02805-3.

Domenech, J., de Britto, M., Velázquez, A., Pastor, S., Hernández, A., Marcos, R., Cortés, C., 2021. Long-term effects of polystyrene nanoplastics in human intestinal Caco-2 cells. Biomolecules 11 (10), 1442. https://doi.org/10.3390/biom11101442.

Foroozandeh, P., Aziz, A.A., 2018. Insight into cellular uptake and intracellular trafficking of nanoparticles. Nanoscale Res. Lett. 13 (1), 339. https://doi.org/10.1186/s11671-018-2728-6.

Fu, Y., Fan, M., Xu, L., Wang, H., Hu, Q., Jin, Y., 2022. Amino-functionalized polystyrene nano-plastics induce mitochondria damage in human umbilical vein endothelial cells. Toxics 10 (5), 215. https://doi.org/10.3390/toxics10050215.

García-Rodríguez, A., Rubio, L., Vila, L., Xamena, N., Velázquez, A., Marcos, R., Hernández, A., 2019. The comet assay as a tool to detect the genotoxic potential of nanomaterials. Nanomaterials (Basel) 10, 1385. https://doi.org/10.3390/nano9101385.

Halimu, G., Zhang, Q., Liu, L., Zhang, Z., Wang, X., Gu, W., Zhang, B., Dai, Y., Zhang, H., Zhang, C., Xu, M., 2022. Toxic effects of nanoplastics with different sizes and surface charges on epithelial-to-mesenchymal transition in A549 cells and the potential toxicological mechanism. J. Hazard. Mater. 430, 128485 https://doi.org/10.1016/j.jhazmat.2022.128485.

He, Y., Li, J., Chen, J., Miao, X., Li, G., He, Q., Xu, H., Li, H., Wei, Y., 2020. Cytotoxic effects of polystyrene nanoplastics with different surface functionalization on human HepG2 cells. Sci. Total Environ. 723, 138180 https://doi.org/10.1016/j.scitotenv.2020.138180.

Ho, Y.T., Kamm, R.D., Kah, J.C.Y., 2018. Influence of protein corona and caveolae-mediated endocytosis on nanoparticle uptake and transcytosis. Nanoscale 10 (26), 12386–12397. https://doi.org/10.1039/c8nr02393j.

Jaroszeski, M.J., Radcliff, G., 1999. Fundamentals of flow cytometry. Mol. Biotechnol. 11 (1), 37–53. https://doi.org/10.1007/BF02789175.

Jeong, J., Im, J., Choi, J., 2024. Integrating aggregate exposure pathway and adverse outcome pathway for micro/nanoplastics: a review on exposure, toxicokinetics, and toxicity studies. Ecotoxicol. Environ. Saf. 272, 116022 https://doi.org/10.1016/j.ecoenv.2024.116022.

Kihara, S., Ashenden, A., Kaur, M., Glasson, J., Ghosh, S., van der Heijden, N., Brooks, A. E.S., Mata, J.P., Holt, S., Domigan, L.J., Köper, I., McGillivray, D.J., 2021. Cellular interactions with polystyrene nanoplastics-the role of particle size and protein corona. Biointerphases 16 (4), 041001. https://doi.org/10.1116/6.0001124.

Kik, K., Bukowska, B., Sicińska, P., 2020. Polystyrene nanoparticles: sources, occurrence in the environment, distribution in tissues, accumulation, and toxicity to various organisms. Environ. Pollut. 262, 114297 https://doi.org/10.1016/j.envpol.2020.114297.

Klingberg, H., Oddershede, L.B., Loeschner, K., Larsen, E.H., Loft, S., Møller, P., 2015. Uptake of gold nanoparticles in primary human endothelial cells. Toxicol. Res. 4 (3), 655–666. https://doi.org/10.1039/C4TX00061G.

Lampitt, R.S., Fletcher, S., Cole, M., Kloker, A., Krause, S., O'Hara, F., Ryde, P., Saha, M., Voronkova, A., Whyle, A., 2023. Stakeholder alliances are essential to reduce the scourge of plastic pollution. Nat. Commun. 14 (1), 2849. https://doi.org/10.1038/s41467-023-38613-3.

Lehner, R., Weder, C., Petri-Fink, A., Rothen-Rutishauser, B., 2019. Emergence of nanoplastic in the environment and possible impact on human health. Environ. Sci. Technol. 53 (4), 1748–1765. https://doi.org/10.1021/acs.est.8b05512.

Leslie, H.A., van Velzen, M.J.M., Brandsma, S.H., Vethaak, A.D., Garcia-Vallejo, J.J., Lamoree, M.H., 2022. Discovery and quantification of plastic particle pollution in

human blood. Environ. Int. 163, 107199 https://doi.org/10.1016/j.envint.2022.107199.
Li, T., Song, X., Zhang, J., Zhao, L., Shi, Y., Li, Z., Liu, J., Liu, N., Yan, Y., Xiao, Y., Tian, X., Sun, W., Guan, Y., Liu, B., 2017. Protection of human umbilical vein endothelial cells against oxidative stress by MicroRNA-210. Oxidative Med. Cell. Longev. 17, 3565613 https://doi.org/10.1155/2017/3565613.
Liu, S., Wu, X., Gu, W., Yu, J., Wu, B., 2020. Influence of the digestive process on intestinal toxicity of polystyrene microplastics as determined by *in vitro* Caco-2 models. Chemosphere 256, 127204. https://doi.org/10.1016/j.chemosphere.2020.127204.
Liu, X., Lu, B., Fu, J., Zhu, X., Song, E., Song, Y., 2021. Amorphous silica nanoparticles induce inflammation via activation of NLRP3 inflammasome and HMGB1/TLR4/MYD88/NF-kb signaling pathway in HUVEC cells. J. Hazard. Mater. 404 (Pt B), 124050 https://doi.org/10.1016/j.jhazmat.2020.124050.
Lu, Y.Y., Li, H., Ren, H., Zhang, X., Huang, F., Zhang, D., Huang, Q., Zhang, X., 2022. Size-dependent effects of polystyrene nanoplastics on autophagy response in human umbilical vein endothelial cells. J. Hazard. Mater. 421, 126770 https://doi.org/10.1016/j.jhazmat.2021.126770.
Lundqvist, M., Stigler, J., Elia, G., Lynch, I., Cedervall, T., Dawson, K.A., 2008. Nanoparticle size and surface properties determine the protein corona with possible implications for biological impacts. Proc. Natl. Acad. Sci. USA 105 (38), 14265–14270. https://doi.org/10.1073/pnas.0805135105.
Paget, V., Dekali, S., Kortulewski, T., Grall, R., Gamez, C., Blazy, K., Aguerre-Chariol, O., Chevillard, S., Braun, A., Rat, P., Lacroix, G., 2015. Specific uptake and genotoxicity induced by polystyrene nanobeads with distinct surface chemistry on human lung epithelial cells and macrophages. PLoS One 10 (4), e0123297. https://doi.org/10.1371/journal.pone.0123297.
Pradel, A., Catrouillet, C., Gigault, J., 2023. The environmental fate of nanoplastics: what we know and what we need to know about aggregation. NanoImpact 29, 100453. https://doi.org/10.1016/j.impact.2023.100453.
Rampado, R., Crotti, S., Caliceti, P., Pucciarelli, S., Agostini, M., 2020. Recent advances in understanding the protein corona of nanoparticles and in the formulation of "stealthy" nanomaterials. Front. Bioeng. Biotechnol. 8, 166. https://doi.org/10.3389/fbioe.2020.00166.
Richter, M., Piwocka, O., Musielak, M., Piotrowski, I., Suchorska, W.M., Trzeciak, T., 2021. From donor to the lab: a fascinating journey of primary cell lines. Front. Cell Develop. Biol. 9, 711381 https://doi.org/10.3389/fcell.2021.711381.
Roshanzadeh, A., Park, S., Ganjbakhsh, S.E., Park, J., Lee, D.H., Lee, S., Kim, E.S., 2020. Surface charge-dependent cytotoxicity of plastic nanoparticles in alveolar cells under cyclic stretches. Nano Lett. 20 (10), 7168–7176. https://doi.org/10.1021/acs.nanolett.0c02463.
Roursgaard, M., Hezareh Rothmann, M., Schulte, J., Karadimou, I., Marinelli, E., Møller, P., 2022. Genotoxicity of particles from grinded plastic items in Caco-2 and HepG2 cells. Front. Public Health 10, 906430. https://doi.org/10.3389/fpubh.2022.906430.
Rubio, L., Marcos, R., Hernández, A., 2020a. Potential adverse health effects of ingested micro- and nanoplastics on humans. Lessons learned from *in vivo* and *in vitro* mammalian models. J. Toxicol. Environ. Health. Part B 23 (2), 51–68. https://doi.org/10.1080/10937404.2019.1700598.
Rubio, L., Barguilla, I., Domenech, J., Marcos, R., Hernández, A., 2020b. Biological effects, including oxidative stress and genotoxic damage, of polystyrene nanoparticles in different human hematopoietic cell lines. J. Hazard. Mater. 398, 122900 https://doi.org/10.1016/j.jhazmat.2020.122900.
Ruenraroengsak, P., Tetley, T.D., 2015. Differential bioreactivity of neutral, cationic, and anionic polystyrene nanoparticles with cells from the human alveolar compartment: robust response of alveolar type 1 epithelial cells. Part. Fibre Toxicol. 12, 19. https://doi.org/10.1186/s12989-015-0091-7.
Ruenraroengsak, P., Novak, P., Berhanu, D., Thorley, A.J., Valsami-Jones, E., Gorelik, J., Korchev, Y.E., Tetley, T.D., 2012. Respiratory epithelial cytotoxicity and membrane damage (holes) caused by amine-modified nanoparticles. Nanotoxicology 6 (1), 94–108. https://doi.org/10.3109/17435390.2011.558643.
Sawyer, L., Grubb, D.T., Meyers, G.F., 2008. Polymer Microscopy. Springer Science and Business Medium, New York. https://doi.org/10.1007/978-0-387-72628-1.
Schneider, M., Stracke, F., Hansen, S., Schaefer, U.F., 2009. Nanoparticles and their interactions with the dermal barrier. Dermato-endocrinology 1 (4), 197–206. https://doi.org/10.4161/derm.1.4.9501.
Setyawati, M.I., Tay, C.Y., Bay, B.H., Leong, D.T., 2017. Gold nanoparticles-induced endothelial leakiness depends on particle size and endothelial cell origin. ACS Nano 11 (5), 5020–5030. https://doi.org/10.1021/acsnano.7b01744.
Shi, X., Wang, X., Huang, R., Tang, C., Hu, C., Ning, P., Wang, F., 2022. Cytotoxicity and genotoxicity of polystyrene micro- and nanoplastics with different size and surface modification in A549 cells. Int. J. Nanomedicine 17, 4509–4523. https://doi.org/10.2147/IJN.S381776.
Sökmen, T.Ö., Sulukan, E., Türkoğlu, M., Baran, A., Özkaraca, M., Ceyhun, S.B., 2020. Polystyrene nanoplastics (20 nm) are able to bioaccumulate and cause oxidative DNA damages in the brain tissue of zebrafish embryos (*Danio rerio*). Neurotoxicology 77, 51–59. https://doi.org/10.1016/j.neuro.2019.12.010.
Son, J., Hong, S.J., Lim, J.W., Jeong, W., Jeong, J.H., Kang, H.W., 2021. Engineering tissue-specific, multiscale microvasculature with a capillary network for prevascularized tissue. Small Methods 5 (10), e2100632. https://doi.org/10.1002/smtd.202100632.
Tavakolpournegari, A., Annangi, B., Villacorta, A., Banaei, G., Martin, J., Pastor, S., Marcos, R., Hernández, A., 2023. Hazard assessment of different-sized polystyrene nanoplastics in hematopoietic human cell lines. Chemosphere 325, 138360. https://doi.org/10.1016/j.chemosphere.2023.138360.
Tirichen, H., Yaigoub, H., Xu, W., Wu, C., Li, R., Li, Y., 2021. Mitochondrial reactive oxygen species and their contribution in chronic kidney disease progression through oxidative stress. Front. Physiol. 12, 627837 https://doi.org/10.3389/fphys.2021.627837.
Vela, L., Villacorta, A., Venus, T., Estrela-Lopis, I., Pastor, S., García-Rodriguez, A., Rubio, L., Marcos, R., Hernández, A., 2023. The potential effects of *in vitro* digestion on the physicochemical and biological characteristics of polystyrene nanoplastics. Environ. Pollut. 329, 121656 https://doi.org/10.1016/j.envpol.2023.121656.
Vila, L., Rubio, L., Annangi, B., García-Rodríguez, A., Marcos, R., Hernández, A., 2017. Frozen dispersions of nanomaterials are a useful operational procedure in nanotoxicology. Nanotoxicology 11 (1), 31–40. https://doi.org/10.1080/17435390.2016.1262918.
Villacorta, A., Rubio, L., Alaraby, M., López-Mesas, M., Fuentes-Cebrian, V., Moriones, O. H., Marcos, R., Hernández, A., 2022. A new source of representative secondary PET nanoplastics. Obtention, characterization, and hazard evaluation. J. Hazard. Mater. 439, 129593 https://doi.org/10.1016/j.jhazmat.2022.129593.
Wang, X., Jia, Z., Zhou, X., Su, L., Wang, M., Wang, T., Zhang, H., 2023. Nanoplastic-induced vascular endothelial injury and coagulation dysfunction in mice. Sci. Total Environ. 865, 161271 https://doi.org/10.1016/j.scitotenv.2022.161271.
Wei, W., Li, Y., Lee, M., Andrikopoulos, N., Lin, S., Chen, C., Leong, D.T., Ding, F., Song, Y., Ke, P.C., 2022. Anionic nanoplastic exposure induces endothelial leakiness. Nat. Commun. 13 (1), 4757. https://doi.org/10.1038/s41467-022-32532-5.
Xu, C., Xu, J., Tang, H.W., Ericsson, M., Weng, J.H., DiRusso, J., Hu, Y., Ma, W., Asara, J. M., Perrimon, N., 2023. A phosphate-sensing organelle regulates phosphate and tissue homeostasis. Nature 617 (7962), 798–806. https://doi.org/10.1038/s41586-023-06039-y.
Xue, J., Zhang, Z., Sun, Y., Jin, D., Guo, L., Li, X., Zhao, D., Feng, X., Qi, W., Zhu, H., 2023. Research progress and molecular mechanisms of endothelial cells inflammation in vascular-related diseases. J. Inflamm. Res. 16, 3593–3617. https://doi.org/10.2147/JIR.S418166.
Yee, M.S., Hii, L.W., Looi, C.K., Lim, W.M., Wong, S.F., Kok, Y.Y., Tan, B.K., Wong, C.Y., Leong, C.O., 2021. Impact of microplastics and nanoplastics on human health. Nanomaterials (Basel) 11 (2), 496. https://doi.org/10.3390/nano11020496.
Yu, Z., Li, Q., Wang, J., Yu, Y., Wang, Y., Zhou, Q., Li, P., 2020. Reactive oxygen species-related nanoparticle toxicity in the biomedical field. Nanoscale Res. Lett. 15 (1), 115. https://doi.org/10.1186/s11671-020-03344-7.
Zhu, X., Wang, C., Duan, X., Liang, B., Genbo, Xu E., Huang, Z., 2023. Micro- and nanoplastics: a new cardiovascular risk factor? Environ. Int. 171, 107662 https://doi.org/10.1016/j.envint.2022.107662.